A NEW APPROACH FOR DETERMINING THE R-CURVE IN DCB TESTS WITHOUT OPTICAL MEASUREMENTS

J. De Gracia*, A. Boyano, A. Arrese, F. Mujika

Materials + Technologies Group

Department of Mechanical Engineering

Polytechnic University College - University of the Basque Country

Plaza de Europa, 1, 20018 San Sebastián, Spain

E-mail: juan.degracia@ehu.es // Tel: +34 943 018665/ +34 688 617 453

Abstract

A new method for obtaining the R-curve point to point by the Double Cantilever Beam test is proposed. Besides the determination of new compliance and energy release rate equations, the analytical model presented leads to calculate the crack length for every pair of load and displacement values, without any optical measurement. In addition, a simple trigonometric approximation is proposed for the calculation of large displacement effects. The approach is checked with experimental results.

Keywords; Delamination; Double Cantilever Beam; Crack length.

1 Introduction

Initiation and propagation of interlaminar cracks is frequently pointed as the most common form of damage in fiber-reinforced laminate composites. Linear elastic fracture mechanics (LEFM) deals with the resistance to delamination by measuring the energy dissipated per unit area of crack growth, that is, the strain energy release rate G.

The Double Cantilever Beam (DCB) test is the most popular method used for determining mode I fracture toughness because of its simplicity and practicality, and has been standardized for carbon fiber reinforced plastic (CFRP) specimens' preparation and test procedures. Furthermore, the application of the compliance-based stability criterion [1] and its experimental verification [2] show stable crack growth for the DCB specimen under displacement controlled loading, which makes it well suited for required measurements. In the test, however, there is a difficulty due to the necessity of measuring the crack length during the process. The standards require a visual measurement of the crack length, which is facilitated by the use of correction fluid on the edges of the specimen and, optionally, by the use of a travelling microscope. In some cases the use of a transparent material facilitates the crack front identification [3]. Nevertheless, sometimes the crack tip is not easy to identify and this can prompt errors in the results.

The data analysis explained in ASTM [4] and ISO [5] standards are based on the change in the compliance, which results in a change of strain energy. Hashemi et al. [6] compared the different data reduction methods for obtaining the critical energy-release rate of fiber composites concluding that a correction for the crack length was necessary in the methods based on the Beam Theory. This is because forces and moments cause deformation in the end region of the DCB, as a consequence of the beam not being perfectly clamped. They developed the Corrected Beam Theory (CBT), providing a correction in the crack length based on a compliance calibration. Williams [7] studied the corrections for large displacement, as well as for end block effects.

Many analytical models have been developed to predict the delamination of the unidirectional fiber reinforced laminated composite DCB specimen. Williams [8] studied the effect of the root flexibility in orthotropic DCB specimens by using a

Timoshenko beam on an elastic foundation, which was an extension of Kanninen´s method for isotropic materials [9, 10]. He concluded that the beam root region in orthotropic specimens acts as a short beam dominated by shear deformation, leading to a large rotation at this place compared to the isotropic case. Whitney [11] used a higher order plate theory to analyze the orthotropic specimen. The shear deformation effect on the energy release rate of delaminated plates was studied by Bruno et al [12], where important contribution was found for the DCB specimen.

Olsson [13] analyzed the displacement of the cracked portion of the specimen from the Classical Beam Theory corrected for shear deformation. He also determined the end displacement caused by the transverse compliance in the un-cracked part and the Saint Venant effects ahead the crack front. Taking into account all these contributions, he used a superposition technique to calculate the overall compliance. Olsson concluded that Williams' solution is slightly stiffer, being Whitney´s model more accurate compared to the Finite Elements solution. Ozdil and Carlsson [14] used Euler–Bernoulli beam on elastic foundation to model the un-cracked region of angle-ply laminated DCB specimens. Kondo [15] studied the DCB specimen utilizing a Timoshenko beam supported by a Winkler foundation, considering that the symmetry of the specimen permits no rotational stiffness at the foundation. Szekrényes [16] presented an improved analysis including Winkler–Pasternak foundation, transverse shear, Saint–Venant effect and crack tip shear deformation. Hamed et al. [17] considered a second-order shear deformation theory to model the DCB specimen. Pavan Kumar et al. [18] used a higher order shear deformation beam theory in terms of quadratic variation for transverse displacement over the thickness. Shokrieh et al. [16] presented a method based on a sixth-order beam theory on a Winkler elastic foundation taking into account both transverse shear and crack tip deformation. However, Olsson [19] reviewed models for

the DCB specimen concluding that the use of energy approaches to incorporate the crack tip compliance or Timoshenko beams on a Winkler foundation are the methods that best fit the FEM results.

Yoshihara et al. [20] introduced a new method for measuring fracture toughness of wood called the Compliance Combination Method. This method uses the longitudinal strain of the top surface of a specimen, measured during the test, to obtain the compliance independently from the crack length. This value allows calculating the crack length and thus, the energy release rate. Gundeson et al. [21] applied both the elastic-plastic fracture mechanics theory and a solution to the J-integral in order to relate fracture toughness with load and angular displacement, being the latter measured during the test.

De Moura et al. [22] proposed a data reduction scheme for wood fracture characterization using the specimen compliance and the crack equivalent concept, avoiding the crack length measurement during propagation. Nevertheless, different initial crack lengths have to be optically measured to obtain root rotation correction. The method estimates the flexural modulus from the initial compliance obtained in the test. Therefore, the initial crack length corrected with a factor to account for the root rotation effects is provided. The crack equivalent concept is introduced to consider the fracture process zone effect at the crack tip. This method has been used in later works [23, 24]-[25] to analyze mode I interlaminar fracture in different composites.

The aim of the present work is to introduce a new method for the determination of the energy release rate without any optical measurement of the crack length. With this purpose, a new model that simplifies the stress distribution on the uncracked part of the specimen is introduced. The crack length is obtained based on the compliance of the model after having determined the elastic properties of the specimen. Furthermore, large

displacements effects are included in a simple manner. Is this way, crack length is defined point to point, and thus a continuous plot of the R-curve can be also determined. In order to check the accuracy of the crack length obtained by DCB, measurements have been also carried out by End Notched Flexure (ENF) tests in the same specimens without crack propagation. For this purpose, the ‘‘Beam Theory including Bending Rotation effects’’ (BTBRs), proposed by Arrese et al. [26] , has been followed.

Nomenclature

a	Delamination length (mm)
a_0	Initial crack length prior to crack propagation (mm)
A	Cross sectional area (mm^2)
B	DCB specimen width (mm)
C	Compliance of the specimen (mm/N)
C_s	System compliance (mm/N)
E_f	Flexural modulus (GPa)
E_3	Tensile modulus in the transversal direction (GPa)
F_1, F_2, F_3	Equivalent point forces for distributed load. (N)
G_{13}	In-plane shear modulus (GPa)
G_I	Strain energy release rate (J/m^2)
h	Laminate half thickness (mm)
I	Second moment of area (mm^4)
k_s	Stiffness of the system (mm/N)
L	Beam length (mm)
M_i	Bending moment at i (N-mm)
Q_i	Shear strength at i (N)

P	Opening load on the DCB specimen (N)
q_1, q_3	Distributed forces in the model (N/m)
U	Strain energy (N-m)
x	Projection of the crack length in the horizontal direction (mm)
x_1, x_2, x_3	Parameters of the distributed forces model (mm)
$\beta_1, \beta_2, \beta_3, \beta_4$	x_1, x_2 and $x_3$dependent parameters
$\gamma_1, \gamma_2, \gamma_3$	x_1 and x_2 dependent parameters
δ_i	Beam displacement at i (mm)
δ_{exp}	Experimental displacement (mm)
δ_{spec}	Specimen displacement (mm)

2 Analytical approach

2.1 Introduction

Fig. 1 shows the configuration of the standardized DCB test. In order to achieve pure mode I, a pre-cracked specimen is loaded at one edge by means of bonded blocks or piano hinges. To determine mode I delamination toughness a compliance-based method is used. Compliance is defined as the ratio of opening displacement of the crack mouth (2δ) to the applied load at that point (P), $C = 2\delta/P$. Having a relationship between the compliance and the crack length, the Strain Energy Release Rate (G_I), which is a measure of fracture toughness, is obtained by differentiating the compliance with respect to the crack length [27].

$$G_I = \frac{P^2 dC}{2Bda} \quad \textbf{(1)}$$

where B is the width of the specimen, a is the crack length and C is the compliance of the specimen.

The crack length a is usually measured visually, and a correction factor is needed in order to take into account the effect of rotation at the crack tip. In this study a new method based on the stiffness of the specimen is presented. Since the configuration is symmetric, only the lower half of the specimen will be considered in further calculations.

2.2 Approximate crack length

The cracked part of the specimen will be modeled as a simple cantilever beam, with the aim of determining an initial approximated crack length (Fig. 2).

According to Engesser-Castigliano theorem, the derivative of the strain energy with respect to the applied force provides the displacement in the direction of the force. The theorem applied to a beam of length L with bending and shear effects is:

$$\delta_i = \frac{\partial U}{\partial F_i} = \int_L \frac{M}{E_f I}\frac{\partial M}{\partial F_i}dx + \int_L \kappa\frac{Q}{G_{13}A}\frac{\partial Q}{\partial F_i}dx \quad \textbf{(2)}$$

Where F_i is the applied force; δ_i is the displacement of the application point of F_i in the same direction; M is the bending moment; Q is the shear force; E_f is the flexural modulus; $G_{13} = G_{12}$ is the shear modulus, assuming transverse isotropy; I is the second moment of area; A is the cross sectional area κ is the shear correction factor which in rectangular section is 6/5.

Taking into account the shear forces and bending moments it results:

$$\delta = \frac{Pa^3}{3E_f I} + \frac{6Pa}{5G_{13}A} \quad \textbf{(3)}$$

Eq. (3) allows defining the compliance as follows:

$$C = \frac{2\delta}{P} = \frac{2a^3}{3E_f I} + \frac{12a}{5G_{13}A} = \frac{2a^3}{3E_f I}\left(1 + \frac{3}{10}\frac{E_f}{G_{13}}\frac{h^2}{a^2}\right) \quad \textbf{(4)}$$

Since the compliance can be determined with the data registered by the test machine, Eq. (3) leads to obtain the crack length by means of an iterative method according to:

$$a_{0_i} = \sqrt[3]{\frac{C}{\left(1 + \frac{3}{10}\frac{E_f}{G_{13}}\frac{h^2}{a_{0_{i-1}}^2}\right)}\frac{3E_f I}{2}} \quad \textbf{(5)}$$

It is worth noting that the crack length given in Eq. (5) is obtained from the displacement of Eq. (3) that does not include the effect of the rotation at the crack tip. The initial crack length a_{0_1} is obtained neglecting shear effects, or in other words assuming that a_{00} is infinite. A similar procedure was followed for obtaining the crack length of an ENF test [26]. Therefore, the value obtained in Eq. (5) can be used as a first approach for the determination of the crack length.

2.3 Interlaminar normal stress distribution ahead of the crack tip

Fig. 3 shows a simplified model with distributed forces based on the results of the models presented by different authors [8-15]. These models present a common shape for the stress distribution ahead of the crack tip, which has been approached to the one caused by two triangular distributed forces $q_1$and q_3. The maximum intensities of the distributed loads are q_{10} and q_{30}, located at sections 1 and 3 respectively.

It is assumed that distributed loads equilibrate the effect of the applied load. Thus, force and moment at the clamped end of the model are null. In spite of the clamped condition is not necessary in the determination of redundant forces, it is necessary for obtaining displacements after applying the unit load method.

The resultant forces of the linear distributions are:

$$F_1 = \frac{q_{10}x_1}{2};\ F_2 = \frac{q_{10}x_2}{2};\ F_3 = \frac{q_{30}x_3}{2} \quad \textbf{(6)}$$

Bending moments and shear forces for the different zones in Fig. 3 are:

$0 < x < x_1$;

$$\begin{cases} M_{x_1} = -F_1 \dfrac{x^3}{3{x_1}^2} \\ Q_{x_1} = -F_1 \dfrac{x^2}{{x_1}^2} \end{cases}$$

$x_1 < x < x_1 + x_2;$

$$\begin{cases} M_{x_2} = \dfrac{F_1}{3x_2x_1}(x^3 - (3x_1 + 3x_2)x^2 + (3{x_1}^2 + 3x_2x_1)x - {x_1}^3 - b{x_1}^2 \\ Q_{x_2} = F_1\left(1 - \dfrac{2x}{x_1} + \dfrac{(x - x_1)^2}{x_2x_1}\right) \end{cases} \quad \textbf{(7)}$$

$x_1 + x_2 < x < x_1 + x_2 + x_3;$

$$\begin{cases} M_{x_3} = -F_1\left(\dfrac{x_2 + x_1}{x_1}x + \dfrac{-{x_2}^2 - 3x_2x_1 - 2{x_1}^2}{3x_1}\right) + F_3\dfrac{(x - x_1 - x_2)^3}{3{x_3}^2} \\ Q_{x_3} = -F_1\dfrac{x_1 + x_2}{x_1} + F_3\dfrac{(x - x_1 - x_2)^2}{{x_3}^2} \end{cases}$$

$x_1 + x_2 + x_3 < x < x_1 + x_2 + x_3 + a;$

$$\begin{cases} M_a = -F_1\left(\dfrac{x_2 + x_1}{x_1}x + \dfrac{-{x_2}^2 - 3x_2x_1 - 2{x_1}^2}{3x_1}\right) + F_3(x - x_1 - x_2 - \dfrac{2x_3}{3}) \\ Q_a = -F_1\dfrac{x_1 + x_2}{x_1} + F_3 \end{cases}$$

Five equations will be considered in order to obtain the dimensions x_1, x_2, x_3, and the forces $F_1$and F_3, since $F_2 = F_1x_2/x_1$.

From static equilibrium it results

$$\sum F_i = 0 \rightarrow F_3 = P + (1 + \frac{x_2}{x_1})F_1 \quad \textbf{(8)}$$

$$\sum M_i = 0 \rightarrow F_1 = \frac{x_1(x_3 + 3a)}{(x_1 + x_2)(x_1 + 2x_2 + 2x_3)} P \quad \textbf{(9)}$$

The other three equations are obtained imposing that displacements at sections 1, 2 and 3 correspond to the transverse strain in the specimen. To determine the effect of the transverse strain, a half of the specimen is replaced by a spring [9]. The stiffness of the spring will be obtained by relating the extension of the spring to the stiffness for a bar (EA/L). In this case A is B times per unit length, and L is half of the beam thickness.

$$k = \frac{2\,E_3\,B}{h} \quad \textbf{(10)}$$

While the displacement in 2 is zero, the value in 1 and 3 is obtained as a function of the point forces defined above.

$$\begin{cases} \delta_1 = \dfrac{-F_1 h}{B x_1 E_3} \\ \delta_2 = 0 \\ \delta_3 = \dfrac{F_3 h}{B x_3 E_3} \end{cases} \quad \textbf{(11)}$$

Displacements at sections 1, 2 and 3 are determined by the Engesser-Castigliano's theorem. In order to calculate the derivatives of bending moments and shear forces that correspond to displacements in 1, 2 and 3 sections, the unit load method is used in the cantilever of Fig. 3. Thus, equating the displacements so obtained with those of Eq. (11) the following expressions are obtained:

$$x_1 = \frac{\sqrt{5E_f \pm 5E_f\sqrt{\left(1 - \frac{36{G_{13}}^2}{5E_f E_3}\right)}}}{\sqrt{6G_{13}}} h \quad \textbf{(12)}$$

$$x_2 = \frac{x_1}{2}\left(-1 + \sqrt{-1 + \frac{10E_f h^2}{3G_{13}{x_1}^2}}\right) \quad \textbf{(13)}$$

$$\frac{7}{60E_f\mathrm{I}}{x_3}^5+\frac{3\gamma_1+9a}{20E_f\mathrm{I}}{x_3}^4+\frac{\gamma_2+6\gamma_1 a}{12E_f\mathrm{I}}{x_3}^3+\left(\frac{\gamma_1\gamma_3+15\gamma_2 a}{60E_f\mathrm{I}}-\frac{2a}{G_{13}A}\right){x_3}^2+$$
$$+\left(\frac{\gamma_1\gamma_3 a}{20E_f\mathrm{I}}-\frac{\gamma_1 a}{G_{13}A}-\frac{6h}{BE_3}\right)x_3-\frac{2h\gamma_1+6ha}{BE_3}=0 \quad \textbf{(14)}$$

Where:

$$\gamma_1=x_1+2x_2;\ \gamma_2={x_1}^2+3x_1x_2+3{x_2}^2;\ \gamma_3={x_1}^2+2x_1x_2+2{x_2}^2$$

Eq.
(12) leads to two possible solutions for the parameter x_1. Since x_2 and x_3 depend on x_1, two different possible stress distributions have been achieved. Comparison to the solutions given by the models proposed by other author [8-15] leads to the choice of the largest value of x_1 for further calculations.

The solution shows that parameters x_1 and x_2 depend only on the mechanical properties of the material and the geometry of the specimen, while x_3 is also a function of the crack length according to Eq.
(14), that has been solved with Mathematica.

Fig. 4 shows the trend in x_3, for T6T/F593 composite tested in the present work, for different values of the thickness h. In all cases a unique real positive solution has been obtained. It can be seen that for each thickness, x_3 remains practically uniform for the usual values of the crack length. Therefore, it can be considered constant for a uniform thickness.

Table 1 shows the values of the parameters for the material studied.

2.4 Displacement at the end of the cracked beam

In the case of the vertical displacement a vertical unit load is applied at the end section of the clamped beam of Fig. 3, in order to obtain the derivatives of shear forces and bending moments. Applying Eq. (2) with the expressions for moments and forces in Eq. (7), and the derivatives obtained by the unit load method, end point displacement δ is:

$$\delta = \frac{1}{3E_f I} P a^3 + \frac{\beta_1}{4E_f I} P a^2 + \left(\frac{1}{AG_{13}} + \frac{2\beta_2 h}{BE_3} + \frac{\beta_3}{12E_f I} \right) P a + \frac{2\beta_4 h}{BE_3} P \quad \textbf{(15)}$$

The rotation at the crack tip (θ_3) can be determined in similar manner, applying a unit moment at section 3 of Fig. 3, being

$$\theta_3 = \frac{P}{12E_f I} (\beta_3 + 3\beta_1 a) \quad \textbf{(16)}$$

Where the factors β_i only depend on the dimensions x_1, x_2, x_3 being:

$$\beta_1 = \frac{{x_1}^2 + 3x_1 x_2 + 4x_1 x_3 + 3{x_2}^2 + 8x_2 x_3 + 5{x_3}^2}{x_1 + 2x_2 + 2x_3}$$

$$\beta_2 = \frac{3}{x_3 (x_1 + 2x_2 + 2x_3)}$$

$$\beta_3 = \frac{{x_1}^2 x_3 + 3x_1 {x_3}^2 + 3x_1 x_2 x_3 + 3{x_2}^2 x_3 + 6x_2 {x_3}^2 + 3{x_3}^3}{x_1 + 2x_2 + 2x_3}$$

$$\beta_4 = \frac{x_1 + 2x_2 + 3x_3}{x_3 (x_1 + 2x_2 + 2x_3)}$$

2.5 Determination of the crack length

Taking into account that Eq. (15) determinates the end point displacement for half model, the Compliance of the DCB specimen is:

$$C = \frac{2\delta}{P} = \frac{2a^3}{3E_f I} + \frac{\beta_1 a^2}{2E_f I} + \frac{2a}{AG_{13}} + \frac{4h\beta_2 a}{BE_3} + \frac{\beta_3 a}{6E_f I} + \frac{4\beta_4 h}{BE_3} \quad \textbf{(17)}$$

It is known that fiber bridging can be responsible for an increasing crack growth resistance during propagation [28, 29]. Nevertheless, this effect was not observed in the specimens tested. Moreover, piano hinges will be used in the tests in order to minimize the dependence of the deformation on the grips applied to load transfer [30].

Eq. (17) can be equated to the experimental value computed directly from the measured load-displacement curve. As the crack length is the only unknown quantity, it can be obtained by means of an iterative or a "goal seek" method.

This procedure allows obtaining the crack length at any point of the test where P and δ are evaluated.

Eq. (17) has been compared with other expressions for the compliance found in the literature [13, 15], achieving very similar results for the material studied.

2.6 Energy release rate

Replacing the derivative of the compliance with respect to the crack length in Eq. (1), G_I can be expressed as follows:

$$G_I = \frac{P^2 a^2}{BE_f I} + \frac{P^2 \beta_1 a}{2BE_f I} + \frac{P^2}{BAG_{13}} + \frac{2h\beta_2 P^2}{B^2 E_3} + \frac{\beta_3 P^2}{12BE_f I} \quad \textbf{(18)}$$

Fiber reinforced composites often show an increasing interlaminar fracture energy during delamination, as observed experimentally. R-curves are frequently used in order to predict accurately the response of the material during damage propagation, and are obtained by plotting G_I against the crack extension.

2.7 Large displacements effect

When testing thin laminates large displacement effects must be taken into account. The analysis carried out by Williams [7, 31] is based on local moments and leads to measure these effects. This analysis is developed by means of elliptical equations, which numerical results are in tabular form for the different values of the end point angle of the deformed beam.

In order to consider this effect, a new approach is proposed. A half of the specimen is shown in Fig. 2, where x is the length measured along the horizontal direction, a is the crack length along the curved specimen; δ is a half of the displacement; s is the secant between the crack tip and the specimen end; and θ is the angle of the secant.

According to Fig. 2:

$$x = s\,cos\theta \tag{19}$$

Therefore,

$$s = x\sqrt{1 + tan^2\theta} = x\sqrt{1 + \frac{\delta^2}{x^2}} \tag{20}$$

Eq. (20) allows obtaining the influence of large displacement on the cracked beam as a function of the previously estimated crack length and deflection. The comparison between this approximation and that of Williams has shown that the differences are under 0.2% for the specimens studied.

3 Experimental

3.1 Materials and apparatus

T6T/F593 prepregs provided by Hexcel Composites, with a 57% volume-content of fiber, were used to produce laminates. The plates were manufactured by hot press molding. Sixteen-layered unidirectional laminates, $[0]_{16}$, were made with a Teflon film introduced during the piling up process in order to make the initial crack.

The specimens were cut with a diamond disc saw, being the nominal thickness and width of the specimens 3 and 15 mm, respectively. The edges of the laminate were discarded for the preparation of the specimens. Piano hinges were bonded to the specimens and tests were performed using a universal testing machine MTS–Insight 10 with a load cell of 250 N. In order to avoid the influence of the resin rich area the specimens were precracked in mode II by a ENF test, increasing the cracked length around 5 mm.

Several specimens have been tested with the aim of validating the method proposed. Nevertheless, results concerning two specimens are included in the present study:

- Specimen 1: It has been subjected to five load-unload cycles in DCB configuration. With the aim of checking the crack lengths obtained by DCB, the specimen has been tested in ENF configuration without crack propagation before the first cycle and after each cycle, applying the BTBR method that provides reliable values of the crack length [26].
- Specimen 2: After having checked the crack length values obtained by DCB and ENF in specimen 1, specimen 2 is tested continuously in DCB configuration, assuming that crack lengths obtained at each point of the test are valid. In this way, it is possible to obtain the R-curve in a continuous manner.

As mentioned previously, fiber bridging has not been observed in any specimen.

3.2 Preliminary tests

For obtaining the elastic properties E_f and G_{13}, the procedure based on three-point bending tests at different spans proposed by Mujika [32] was used, resulting in a longitudinal flexural modulus of 116 GPa and a shear modulus of 4 GPa. Bending tests were done for each specimen in the uncracked zone, at five different spans.

Specimen displacement (δ_{spec}) was determined from load-displacement curves. The experimental displacement (δ_{exp}) is the addition of the specimen displacement and the displacement due to the system compliance.

$$\delta_{exp} = \delta_{spec} + C_s P \rightarrow \delta_{spec} = \delta_{exp} - C_s P \quad \textbf{(21)}$$

In order to analyze system compliance, a thin steel plate with bonded piano hinges was tested five times as a DCB specimen. As the deformation of the plate is negligible, the slope of the obtained load-displacement curves can be considered to be the effect of the system compliance. The average value obtained for the stiffness of the system was $C_s = 201x10^{-5}\ mm/N$.

C_s includes the compliance effects concerning the different parts of the testing system:

- Piano hinges bonded to the specimen.
- Load cell.
- Testing machine frame.

3.3 Determination of the crack length

In order to determine the crack length the DCB tests were carried out in accordance with the ISO standards [5]. As explained previously, 5 load-unload cycles with crack advance have been carried out in specimen 1, which are shown in Fig. 5.

Load and displacement values obtained from DCB tests have been exported to a spreadsheet where both the experimental compliance and the analytic compliance defined by means of the presented method are calculated point to point in the range of the test. To obtain a first approach of the analytic compliance, it is required to have the initial value of the crack length given in Eq. (5).

After that, a goal seeking method is used to find the crack length by equating both the experimental compliance and the one determined by Eq.(17), allowing the modification

of the initial crack length. Finally, the effects of large displacements explained in section 2.7. are taken into account to obtain the definitive value of the crack length. This process leads to achieve a continuous plot of the crack and therefore the Energy Release Rate along the test can be determined. Fig. 6 shows the effects of the large displacements in specimen 1 for ratios $\mathbf{2\delta/a}$ > 30%. There is a maximum difference of 5 mm between the curves due to the above mentioned effect.

Before the first load-unload cycle and after each one a ENF test without crack advance has been carried out with the aim of determining the real crack length, following the methodology based on BTBR approach[26]. Thus, crack lengths obtained by ENF tests have been used for checking the values obtained by DCB in the same specimen.

Fig. 7 shows the continuous plot of crack lengths obtained by DCB in the five load-unload cycles and the discrete values measured by BTBR every time the test is stopped for specimen 1. a_0 to a_5 are the values measured by ENF tests, and correspond to the initial crack length in each load cycle. The comparison of results obtained by DCB and ENF for different crack lengths in specimen 1 show the capability of the proposed method for obtaining the crack length in a DCB test.

After having validated the crack length determination procedure presented, specimen 2 has been tested without stopping the test. Fig. 8 illustrates the determined crack growth for this specimen.

3.4 Resistance curves

Interlaminar fracture energy is experimentally observed to increase during the delamination process. The R-curve for laminated composite materials shows a monotonically increasing G_{Ic} value in the first few millimeters of crack extension which then stabilizes with further crack growth. Unless fiber bridging is the primary reason for this behavior other effects may be involved in the shape of a resistance curve [33].

Fig. 9 shows the load-displacement graph and the R-curve obtained by Eq. (18), for specimen 1. Zones 1 to 5 correspond to the five load-unload cycles. Some discontinuities (A_1 to A_3) are observed in the graphs. Theoretically, the crack growth proceeds slowly and continuously in infinite small increments. Nevertheless, uneven increments take place when real tests are carried out. These little crack growth jumps produce load drops, which are usually followed by arrest. In this phase, the load increases to a local maximum before continuing the delamination growth [5].
Similar behavior has been observed in the graphs for specimen 2. Fig. 10 shows the Load-displacement graph and the R-curve for this latter specimen. The meaning of the points marked in Fig. 10 is:

NL: Deviation from Linearity. It is assumed that delamination starts to grow from the tip of the initial crack. An initiation value for G_{Ic} should be calculated from this point.

B_1, B_2: Points where the load drops abruptly.

C_1, C_2: Points where the load increases without crack growth after unstable propagation.

The drops showed in the R-curve are caused by the above mentioned drops in load-displacement curve. The crack length increases unstably, provoking the drop in the R-curve. After that the load increases reaching a local maximum before the crack starts to propagate again. The ISO standard [5] states that the points where the crack growth is arrested should be excluded, nevertheless in the presented work all the points are plotted in order to show the complete behavior of the fracture process.

4 Summary and conclusions

A new analytical model regarding the compliance in a DCB specimen has been presented. Besides shear and system compliance effects, large displacements have been taken into account. By means of this approach, an experimental procedure for the point-to-point determination of the R-curve has been proposed. The basic aspect of the procedure is the determination of the crack length based on the compliance of the specimen. Results obtained for the compliance agree with those obtained by other authors. The experimental results obtained for the crack length have been validated by ENF tests with the BTBR method. The point to point plot of the R-curve leads to analyze the real behavior of the specimen, including phases of unstable delamination growth.

The presented method allows a continuous plot of the R-curve without the need of any optical measurement. This aspect is interesting, among others, for carrying out DCB tests in a temperature chamber.

References

[1] T. Anderson, Fracture Mechanics-Fundamentals and Applications 3rd edn., Taylor & Francis Group, 2005.

[2] A. Szekrényes, «Crack stability of fracture specimens used to test unidireccional fiber reinforced material,» *Experimental Mechanics,* vol. 50, pp. 473-482, 2010.

[3] A. Szehrényes, «Prestressed fracture specimen for delamination testing of composites,» *International Journal of Fracture,* nº 139, pp. 213-237, 2006.

[4] ASTM, «Standard D5528-94a, Standard Test Method for Mode I Interlaminar Fracture Toughness of Unidirectional Continuous Fiber Reinforced Polymer Matrix Composites,» Philadelphia, 1994.

[5] ISO, « 15024, Fiber-reinforced Plastic Composites – Determination of Mode I Interlaminar Fracture Toughness, GIc, for Unidirectionally Reinforced Materials,» (2001.

[6] S. Hashemi, A. J. Kinloch y J. G. Williams, «Corrections needed in double-cantilever beam tests for assessing the interlaminar failure of fibre-composites,» *Journal of Materials*

Science Letters, vol. 8, pp. 125-129, 1989.

[7] J. G. Williams, «Large displacement and end block effects in the "DCB" interlaminar test in modes I and II,» *Journal of Composite Materials,* vol. 21, pp. 330-347, 1987.

[8] J. G. Williams, «End corrections for orthotropic DCB specimens,» *Compos Sci Technol,* vol. 35, nº 4, pp. 367-376, 1989.

[9] M. F. Kanninen, «A dynamic analysis of unstable crack propagation and arrest in the DCB test specimen,» *International Journal of Fracture.,* vol. 10, nº 3, pp. 415-430, 1974.

[10] M. F. Kanninen, «An augmented double cantilever beam model for studying crack propagation and arrest,» *International Journal of Fracture,* vol. 9, nº 1, p. 83.92, 1971.

[11] J. M. Whitney, «Stress analysis of the double cantilever beam specimen,» *Compos Sci Technol,* vol. 23, p. 201–219, 1985.

[12] D. Bruno y F. Greco, «Mixed mode delamination in plates: a refined approach,» *International Journal of Solids and Structures,* vol. 38, pp. 9149-9177, 2001.

[13] R. Olsson, «A simplified improved beam analysis of the DCB specimen,» *Compos Sci Technol,* vol. 43, p. 329–338, 1992.

[14] F. Ozdil y L. Carlsson, «Beam analysis of angle-ply laminate DCB specimens,» *Composites Science and Technology,* vol. 59, pp. 305-315, 1999.

[15] K. Kondo, «Analysis of double cantilever beam specimen,» *Advanced Composite Materials,* vol. 4, nº 4, pp. 355-366, 1995.

[16] M. M. Shokrieh, M. Heidari-Rarani y M. R. Ayatollahi, «Interlaminar fracture toughness of unidirectional DCB specimens: A novel theoretical approach,» *Polymer Testing,* vol. 31, p. 68–75, 2012.

[17] M. Hamed, A. Nosier y G. Farrahi, «Separation of delamination modes in composite beams with symmetric delaminations,» *Materials and Design,* vol. 27, pp. 900-910, 2006.

[18] D. V. T. G. Pavan Kumar y B. K. Raghu Prasad, «Analysis of unidirectional (0°) fiber-reinforced laminated composite double cantilever beam specimen using higher order beam theories,» *Engineering Fracture Mechanics,* vol. 75, pp. 2156-2174, 2008.

[19] R. Olsson, «On improper foundation models for the DCB,» de *16th International Conference on Composite Materials*, 2007.

[20] H. Yoshihara y T. Kawamura, «Mode I fracture toughness estimation of wood by DCB test,» *Composites: Part A,* vol. 37, p. 2105–2113, 2006.

[21] J. D. Gunderson, J. F. Brueck y A. J. Paris, «Alternative test method for interlaminar fracture toughness of composites,» *Int J Fract,* p. 273–276, 2007.

[22] M. F. S. F. De Moura, J. J. L. Morais y N. Dourado, «A new data reduction scheme for mode I wood fracture characterization using the double cantilever beam test,» *Engeneering fracture mechanics,* vol. 75, pp. 3852-3865, 2008.

[23] M. F. S. F. De Moura, R. D. S. G. Campilho y J. P. M. Gonçalves, «Crack equivalent concept applied to the fracture characterization of bonded joints under pure mode I loading,» *Composites Science and Technology,* vol. 68, p. 2224–2230, 2008.

[24] M. F. S. F. De Moura, R. D. S. G. Campilho, A. M. Amaro y P. N. B. Reis, «Interlaminar and intralaminar fracture characterization of composites,» *Composite Structures,* vol. 92, p. 144–149, 2010.

[25] J. J. L. Morais, M. F. S. F. De Moura, F. A. M. Pereira, J. Xavier, N. Dourado, D. M. I. R y J. M. T. Azevedo, «The double cantilever beam test applied to mode I fracture characterization of cortical bone tissue,» *Journal of the Mechanical Behavior of Biomedical Materials,* vol. 3, pp. 446-453, 2010.

[26] A. Arrese, N. Carbajal, G. Vargas y F. Mujika, «A new method for determining mode II R-curve by the End-Notched Flexure test,» *Eng. Fract. Mech,* vol. 77, nº 1, pp. 51-70, 2010.

[27] G. R. Irwin y J. A. Kies, «Critical energy release rate analysis of fracture strengthof large welded structures,» *Welding Journal,* vol. 33, pp. 193-198, 1954.

[28] V. Tamuzs, S. Tarasovs y U. Vilks, «Progressive delamination and fiber bridging modeling in double cantilever beam composite specimens,» *Engineering Fracture Mechanics,* vol. 68, nº 5, pp. 513-525, 2001.

[29] A. Szekrényes, «Advanced beam model for fiber-bridging in unidirectional composite double-cantilever beam specimens,» *Engineering Fracture Mechanics,* vol. 72, nº 17, pp. 2686-2702, 2005.

[30] J. Viña, A. Argüelles, A. López, V. Mollón y J. Bonhomme, «Influence of the Loading System on Mode I Delamination Results in Carbon–Epoxy Composites,» *Experimental Techniques,* vol. 38, nº 1, pp. 53-58, 2014.

[31] J. G. Williams, "Fracture Mechanics of Anisotropic Materials," in *Composite Materials Series, sixth volume: Application of Fracture Mechanics to Composite Materials*, Elsevier Science Publishers, 1989, pp. 3-38.

[32] F. Mujika, «On the effect of shear and local deformation in three-point bending tests,» *Polym Test,* vol. 26, pp. 869-877, 2007.

[33] M. Hojo, K. Kageyama y K. Tanaka, «Prestandardization study on mode I interlaminar

fracture toughness test for CFRP in Japan,» *Composites,* vol. 26, nº 4, pp. 243-255, 1995.

TABLE CAPTIONS

Table 1.- *Parameters* $\boldsymbol{x_1, x_2, x_3}$ *for T6T/F593* ($\boldsymbol{h = 1.5}$)

$x_1(mm)$	$x_2(mm)$	$x_3(mm)$
9,95	0,19	1,31

Table 1.- *Parameters* x_1, x_2, x_3 *for T6T/F593* ($h = 1.5$)

FIGURE CAPTIONS

Fig. 1. *DCB specimen*

Fig. 2. *Lower half of the DCB specimen*

Fig. 3. *Distributed force along the beam*

Fig. 4. *Variation of* $\boldsymbol{x_3}$ *with the crack length (h=1, 1.5, and 2mm)*

Fig. 5. *Load-Displacement plot of specimen 1.*

Fig. 6. *Effects of Large Displacements (Specimen 1)*

Fig. 7. *Calculated versus measured crack length in specimen 1*

Fig. 8. *Calculated crack length in specimen 2*

Fig. 9. *(a) Load-Displacement plot and (b) R-curve in specimen 1*

Fig. 10. *(a) Load-Displacement plot and (b) R-curve for specimen 2*

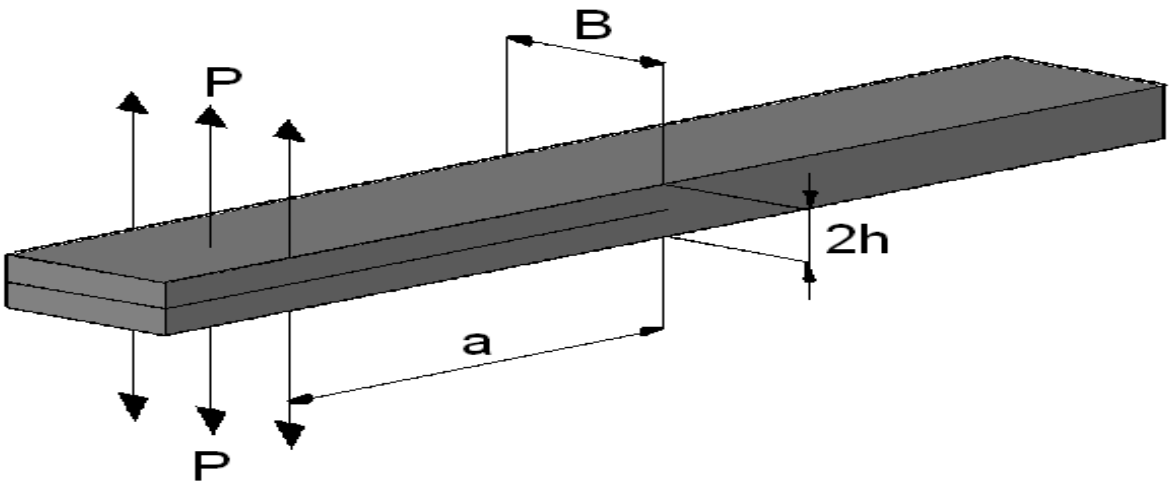

Fig. 1. *DCB specimen*

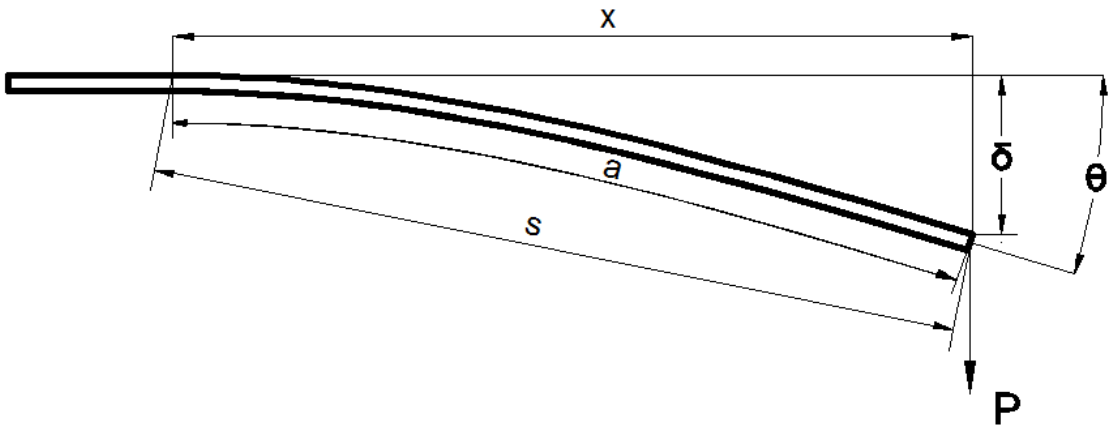

Fig. 2. *Lower half of the DCB specimen*

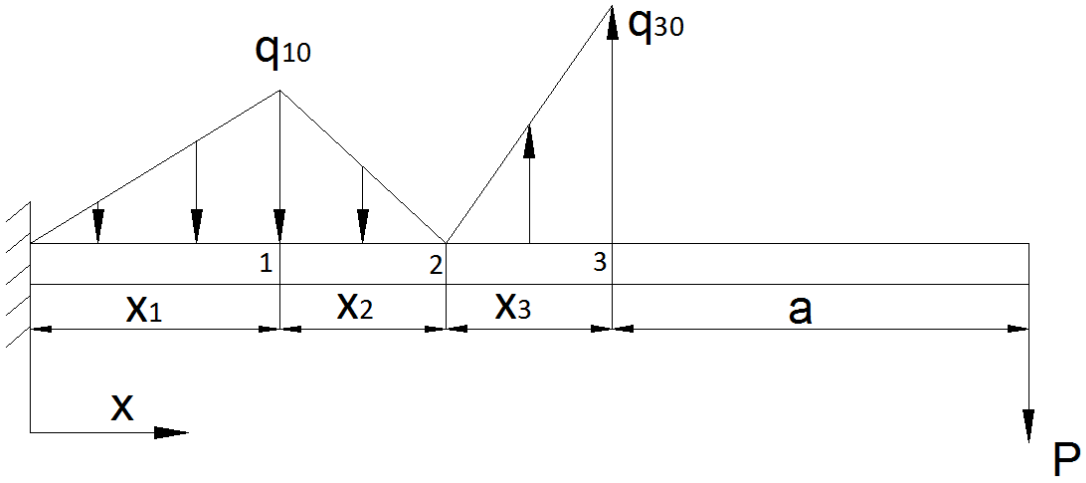

Fig. 3. *Distributed force along the beam*

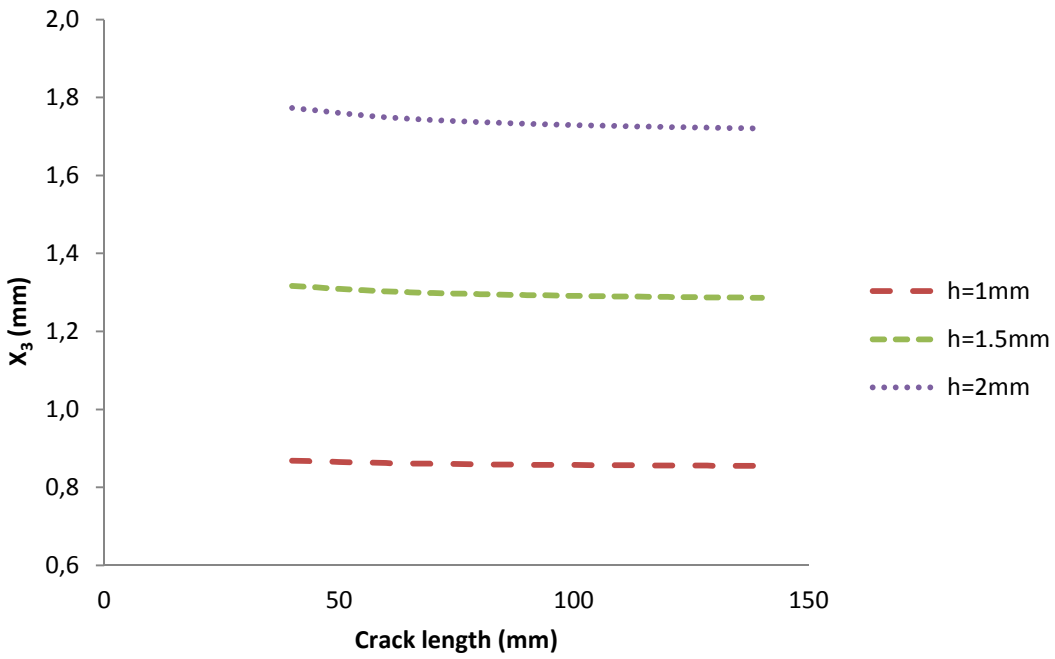

Fig. 4. *Variation of* $\boldsymbol{x_3}$ *with the crack length (h=1, 1.5, and 2mm)*

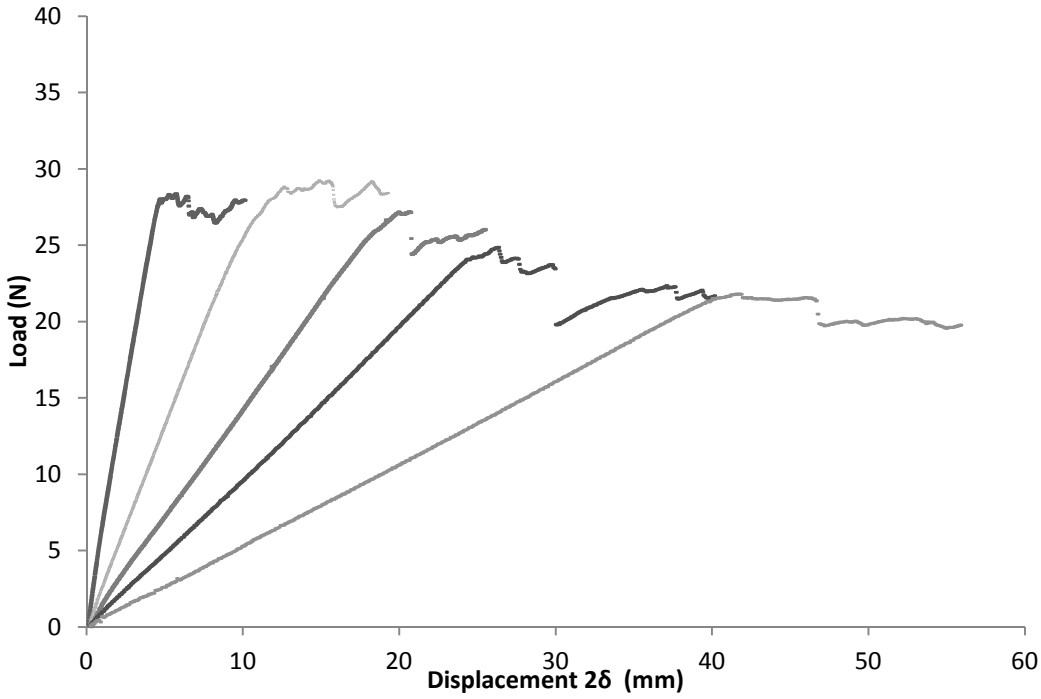

Fig. 5. *Load-Displacement plot of specimen 1.*

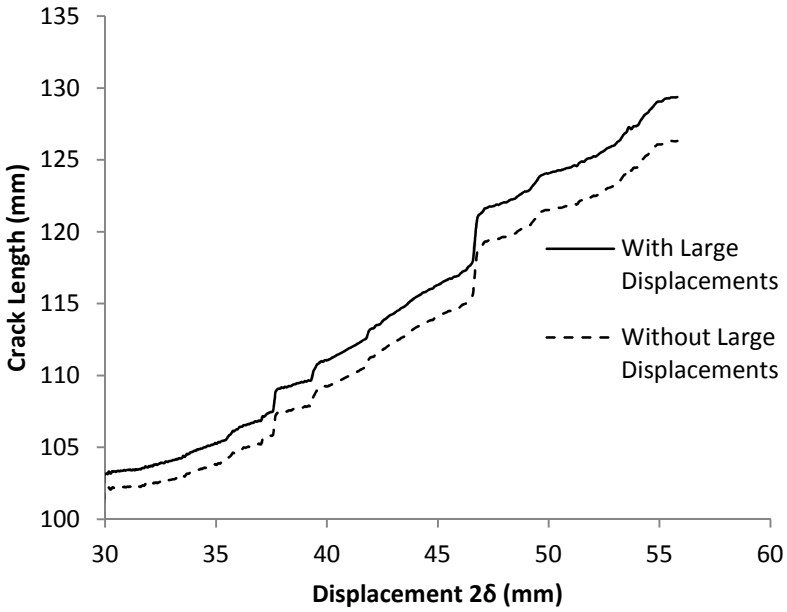

Fig. 6. *Effects of Large Displacements (Specimen 1)*

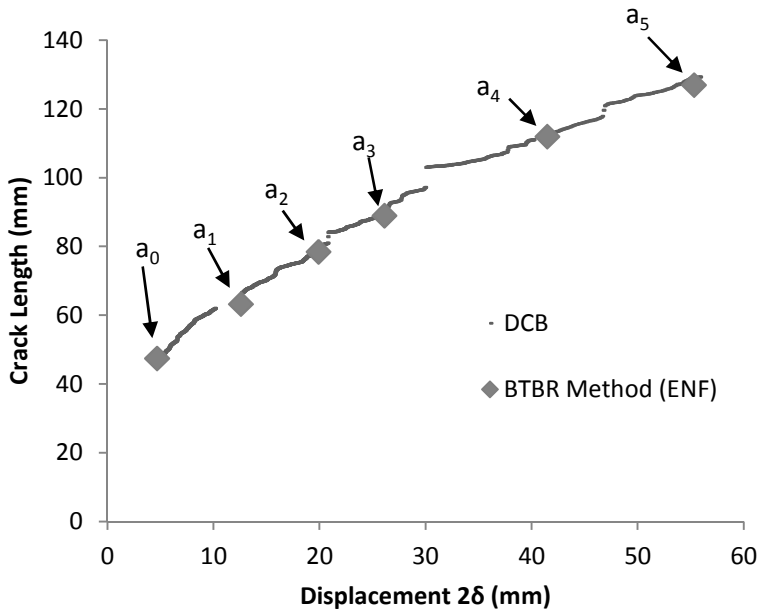

Fig. 7. *Calculated versus measured crack length in specimen 1*

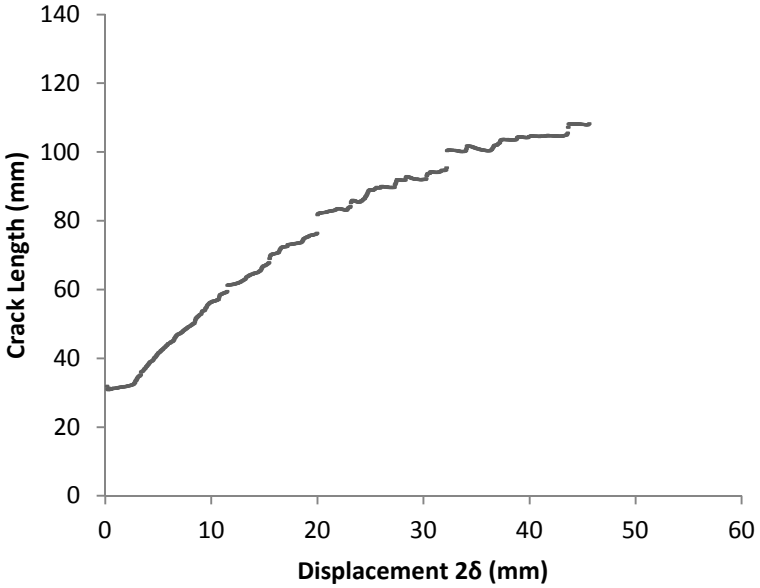

Fig. 8. *Calculated crack length in specimen 2*

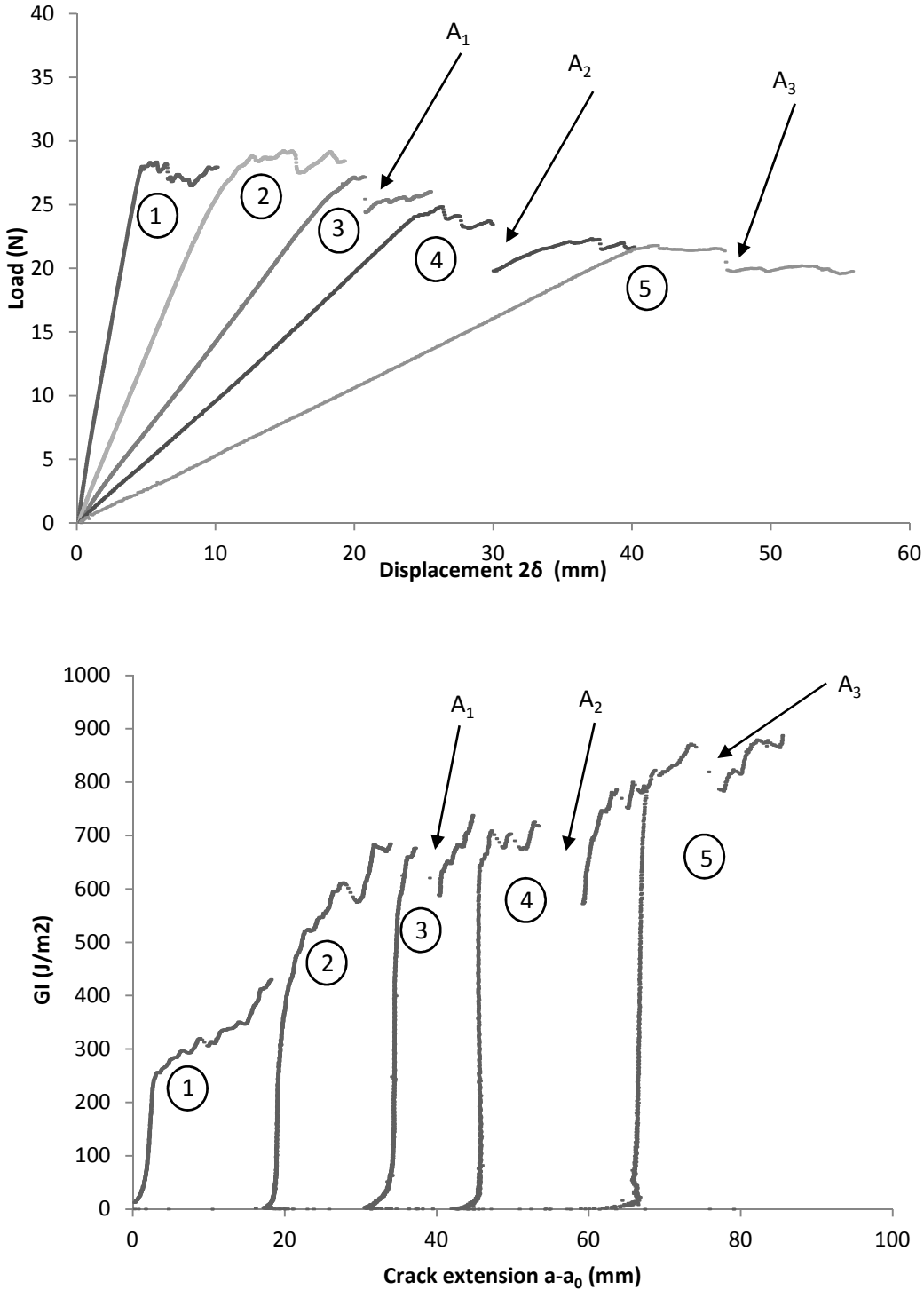

Fig. 9. *(a) Load-Displacement plot and (b) R-curve in specimen 1*

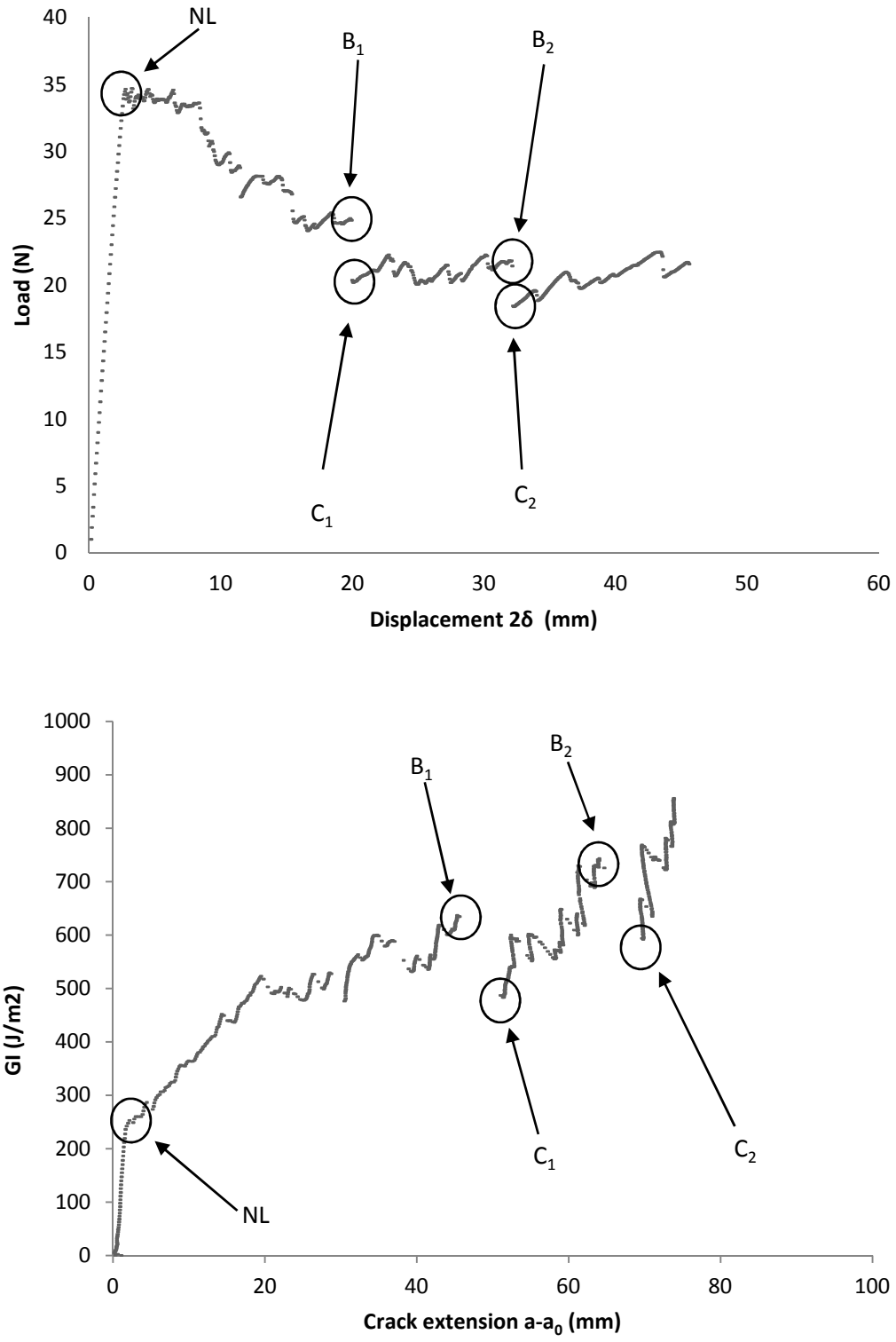

Fig. 10. *(a) Load-Displacement plot and (b) R-curve for specimen 2*